PHYSICAL REVIEW C VOLUME 23, NUMBER 5 MAY 1981

True absorption and scattering of pions on nuclei

D. Ashery, I. Navon, and G. Azuelos*
Physics Department, Tel Aviv University, Israel

H. K. Walter and H. J. Pfeiffer†
Laboratorium fur Hochenergiephysik der Eidgenössische Technische Hochschule, CH-5234, Villigen, Switzerland

F. W. Schlepütz
Physikinstitut der Universität Zürich, CH-8001, Zürich, Switzerland
(Received 28 July 1980)

The cross section for true absorption of pions in nuclei was obtained from experiments at 85, 125, 165, 205, 245, and 315 MeV for positive pions and at 125 and 165 MeV for negative pions. The results are compared with theoretical calculations. The inclusive pion scattering angular distribution was also measured, and the results indicate that quasifree scattering plays an important role for backward scattering. The total pion-nucleus cross section is decomposed into its major channels: elastic scattering, inclusive inelastic scattering, true absorption, and single charge exchange, as a function of pion energy and charge. For light nuclei, the true absorption cross section has a strong energy dependence, reflecting the shape of the (3,3) resonance. The A dependence of the true absorption cross section is much stronger than that of the inclusive inelastic scattering.

[NUCLEAR REACTIONS Li, C, Al, Fe, Nb, Bi ($\pi^{\pm}, \pi'$); measured $\sigma(\theta_{\pi'})$, E_{π^+} = 85, 125, 165, 205, 245, and 315 MeV, E_{π^-} = 125, 165 MeV; deduced $\sigma_{\text{inelastic}}$, $\sigma_{\text{absorption}}$; decomposition of σ_{tot}.]

I. INTRODUCTION

The pion nucleus total cross section was studied systematically in recent years over the 3:3 resonance region.[1] At the same time, the elastic scattering of pions from nuclei was studied, and methods to calculate this process were developed that give satisfactory agreement with the data at these energies.[2,3] From these results, the pion-nucleus reaction cross section is deduced. There is, however, very little information as to how the reaction cross section is decomposed into its major channels: the inelastic scattering (to bound and unbound final states), single and double charge exchange, and pion absorption (where there are no pions in the final state). This information is important not only for understanding the pion nucleus reaction cross section but also for interpretation of the elastic scattering. The problem of how to deal with true absorption in the analysis of elastic scattering has not yet been completely solved[4]; and experimental information on the true absorption cross section will be an important contribution to the solution of this problem. Several theoretical calculations exist[5-9] where the true absorption cross section is calculated. There have also been suggestions to decompose the imaginary part of the pion-nucleus optical potential into absorptive and scattering components[7] or to separate the pion mean free path into such components.[7,10] The lack of sufficient experimental data made it difficult to test the theoretical results and to better understand the behavior of the reactive content of the pion-nucleus interaction.

Previous experimental data on pion absorption in nuclei come predominantly from studies of pionic atoms where the absorption probability is obtained through measurements of the atomic level width. Through parametrization of the optical potential, it is possible to use these widths to predict the cross sections for pion absorption in flight, and this procedure was, in fact, used by Stricker *et al.*[9] up to the (3, 3) resonance region. However, there are many differences between the absorption of pions at bombarding energies near the 3:3 resonance and that of pions at rest, so that separate studies are necessary. The absorption of pions in flight was studied systematically on the deuteron,[11] where this reaction may be regarded as an "elementary" absorption process. However, due to the low deuteron density and the availability of absorption channels and mechanisms in nuclei which do not exist for the deuteron, it is difficult to extrapolate the results from the deuteron to heavy nuclei.[12] Some measurements were done on carbon.[13,14] Many studies of particle and gamma spectra, emitted following pion interaction with nuclei, showed that pion absorption must play an important role in this interaction, but these studies were not able to produce quantitative measurements of the absorption cross sections. From the point of view

of the pion-nucleus interaction, the process of inclusive inelastic scattering and that of true absorption should not be treated separately. Since these two reactions turn out to be of comparable magnitude, and together exhaust over 80% of the reaction cross section, they are expected to be coupled to each other. It is, therefore, advantageous to treat them simultaneously.

In order to obtain this necessary information on these reaction, we carried out a systematic study of pion inclusive scattering and absorption reactions at bombarding energies from 85 to 315 MeV for positive pions and at 125 and 165 MeV for negative pions. The measurements were done on six target nuclei, ranging from ^{7}Li to ^{209}Bi. A small part of the results was published earlier.[15–19]

II. EXPERIMENTAL PROCEDURE

The absorption cross sections were obtained by combining the results of two experiments carried out at the SIN accelerator. The incident pion energies were 85, 125, 165, 205, 245, and 315 MeV for positive pions and 125 and 165 MeV for negative pions. Natural targets of Li, C, Al, Fe, Nb, and Bi of thicknesses 0.59, 1.88, 2.28, 2.53, 4.36, and 4.69 g/cm^2, respectively, were used.

The first experiment was done using a standard transmission technique of the kind used for measurements of total cross sections. The pion beam hit the target after passing through two plastic scintillators used to monitor the beam flux [Fig. 1(a)]. The target was fitted into a 5×5 cm^2 hole in the center of a large plastic scintillator. The beam monitoring and data taking was done requiring anticoincidence with this collimating scintillator and coincidence with the two scintillators on the beam axis. This system ensured that all the monitored beam actually hit the target. Protons present in the beam were eliminated by degraders positioned inside the beam transport channel. Muon and electron contaminations in the beam were measured by time of flight. Five plastic scintillation counters of a disk shape were positioned on the beam axis behind the target position. The counters covered the solid-angle range of 0.1–0.7 sr, and, by changing the distance from the target, the measurements were taken at nine different solid angles for Li, C, Al, and Fe and thirteen for Nb and Bi. These detectors were used to measure the number of charged pions removed from the incident flux by the target. Three processes can remove charged pions from the incident flux:

(a) pion absorption in the target;
(b) single charge exchange in the target;
(c) scattering of charged pions (elastic and inelastic, including double charge exchange) to angles larger than Ω, the solid angle subtended by the disk counter.

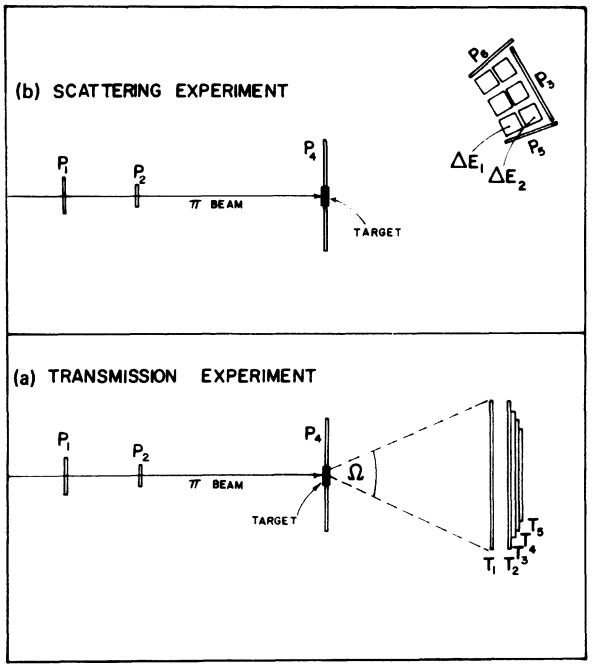

FIG. 1. Schematic diagram of experimental setups. P_i and T_i are scintillation counters.

Denoting the cross sections for these processes by σ_{abs}, σ_{cx}, and $\int_{\Omega}^{4\pi}(d\sigma_{sc}/d\Omega)d\Omega$, respectively, the result of the transmission experiment is the sum of these cross sections:

$$\sigma_{tr}(\Omega) = \frac{1}{n_t} \ln \frac{N(0)}{N(t)} = \sigma_{abs} + \sigma_{cx} + \int_{\Omega}^{4\pi} \frac{d\sigma_{sc}}{d\Omega} d\Omega . \quad (1)$$

Here n_t is the number of target nuclei, and $N(t)$ and $N(0)$ are the number of counts in the detector with and without a target in the beam, respectively.

In the second experiment the differential scattering cross section was measured. Beam monitoring, proton elimination, and contamination measurement were done as in the transmission experiment. The outgoing pions were measured by three telescopes, each consisting of two cubes 5×5×5 cm^3 of plastic scintillator, placed at a distance of 55 cm from the center of the target and separated by 10° [Fig. 1(b)]. Positive pions were discriminated against protons and heavier particles using two, partially overlapping, methods:

(a) Fast pions that passed through the first detector of a telescope were identified by the combination of their energy losses in the detectors ($\Delta E_1 - \Delta E_2$). Particles that passed through both detec-

tors were tagged by a scintillator positioned behind the telescopes.

(b) Slow positive pions which stopped in a telescope were identified and separated from protons by detecting the signal produced by muon decay that follows the pion decay.

The overlap group consisted of the pions that stopped in the second detector. It is important to note that the second method, which can be used only for positive pions, was needed only for those pions that stopped in the first detector ($E_\pi < 22$ MeV). These amounted to only a small fraction, typically 6%, of the whole spectrum. Negative pions that stopped in the first detector were not identified. This was corrected for by assuming that approximately the same fraction of negative and positive pions were stopped in the first detector. The results are not sensitive to this assumption because the correction is small. The telescopes were, therefore, sensitive to the whole range of pion energies present in this experiment. Background measurements were taken with the target removed. The collimating detector mentioned above reduced the background considerably by rejecting muons originating from pion decay along the beam path. As a result, the counting rates with target out were typically 5–10% of the rates with target. From the number of outgoing pions detected at each angle, the differential scattering cross section was obtained over the angular range of 13°–150° in steps of 5°–10° with angular resolution of 5.2°. The absolute 0° angle was checked both by measuring left-right symmetry of the scattered pion cross section and by finding the position of maximum rate when the telescopes were placed in the beam. Both methods gave the same results. The dead time in the measurements was typically 1%. The muon and electron contamination was in the range of 1–7%, depending on pion energy and charge, but reached 22% at 125 MeV π^-. The detection inefficiency of the telescopes, due to pions undergoing reactions in the front scintillator, was measured to be typically 8%. Pions undergoing reactions in the back scintillator of the telescope are still detected and identified as pions. Corrections of the order of 1–5% were also applied to account for loss of pions in the target due to secondary reactions and stopping of very low energy pions in the target. These corrections are bombarding energy, target, and angle dependent. More experimental details are given in Ref. 20.

III. RESULTS

Angular distributions of the scattered pions (integrated over their energies) are shown in Fig. 2 for positive pions at a bombarding energy of 165 MeV. The general features of the angular distributions are quite similar at all the bombarding energies. The errors in each point of the distribution vary between 2% and 8%, including statistical and angle-dependent systematic errors. The statistical errors are less than 3%. The systematic errors come from the uncertainties in some of the corrections discussed in the previous section, and are angle dependent because of variations in the

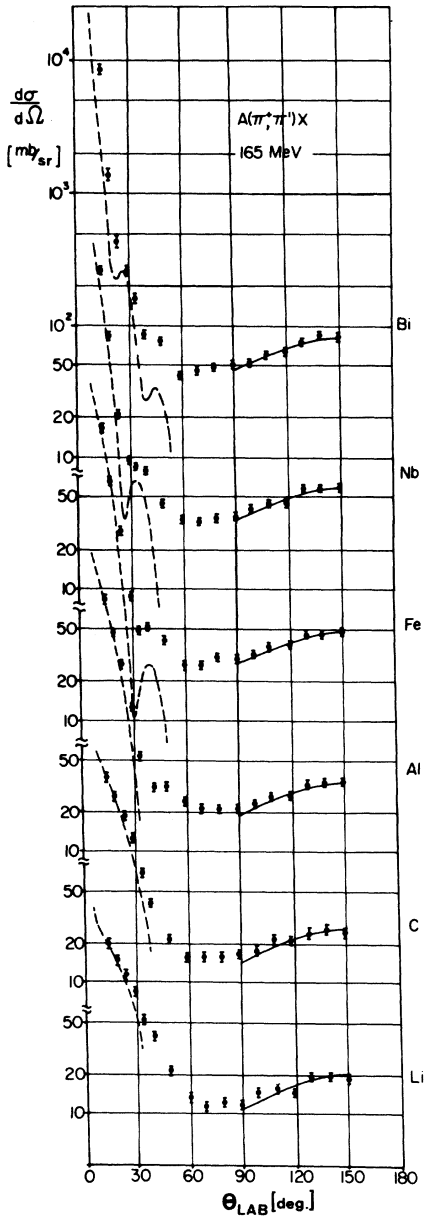

FIG. 2. Differential scattering cross section of 165 MeV π^+ on nuclei. The dashed lines at forward angles are the result of elastic scattering calculations. The solid lines at backward angles is the free $(\pi^+ + p) + (\pi^+ + n)$ cross section normalized to the data.

scattered pion energy spectrum with angle. In addition, there is an angle-independent uncertainty in the absolute normalization, resulting from beam-counting and solid angle determination, which is estimated to be 7%. In order to verify the absolute normalization of the experiment, measurements were taken with a CH_2 target, at all the bombarding energies. After subtracting from the results of these measurements the contribution due to carbon (which is measured separately), we obtain the cross sections for π^+-p scattering, and they are found to agree within 10% with previous measurements[21] of this process.

The measured angular distribution was then integrated over the solid angle complementary to Ω [Ω is the solid angle subtended by the disk counters in the transmission experiment; see Eq. (1)]. Although in this process the differential cross section had to be extrapolated to the region 150°–180°, the result of the integration is insensitive to this extrapolation because the cross section at backward angles is slowly varying and is multiplied by $\sin\theta$ in the integration. The results of the integrations are subtracted from the corresponding values of $\sigma_{tr}(\Omega)$ [Eq. (1)]. Ideally, this difference should be Ω independent and equal to $\sigma_{abs} + \sigma_{cx}$. In practice, the results of transmission measurements include not only pions scattered into the disk counters, but also protons and other charged particles which result from various reactions. This contribution vanishes in the limit $\Omega = 0$. Therefore, in order to obtain $\sigma_{abs} + \sigma_{cx}$, the value of

$$\sigma^*(\Omega) = \sigma_{tr}(\Omega) - \int_{\Omega}^{4\pi} \frac{d\sigma_{sc}}{d\Omega}\, d\Omega$$

is taken as a function of Ω and extrapolated to $\Omega = 0$.

Two such typical extrapolations are shown in Fig. 3. It is characteristic of the measurements with negative pions that the results of the subtraction are almost Ω independent, since the number of emitted protons is small. With positive pions there is a larger slope, but it is not very steep. The errors in the values of $\sigma^*(\Omega)$ come from the contributions of the two measurements—which are partly correlated—and uncertainty in matching the angles. Linear and quadratic fits to the results were used in order to perform the extrapolation to $\Omega = 0$ that yield the value of $\sigma_{abs} + \sigma_{cx}$. Since the quality of the two fits was comparable and there was no *a priori* reason to prefer one of them, the final value of $\sigma_{abs} + \sigma_{cx}$ was taken as the average of the results of the two extrapolations. The difference was taken as the contribution of the extrapolation to the error in the final result. In addition to that, the errors, correlated and uncorrelated, from the two experiments are taken in order to obtain the combined error in the result. Typically, the errors from the extrapolation were 5–10% and the final errors 10–15%. The contribution from the $(\pi, 2\pi)$ reaction at bombarding energies above 200 MeV was estimated from $H(\pi, 2\pi)$ data[22] multiplied by N_{eff} (see Sec. IV A). The result was of the order of 1% of the scattering cross section, and hence neglected. The results of $\sigma_{abs} + \sigma_{cx}$ are listed in Table I.

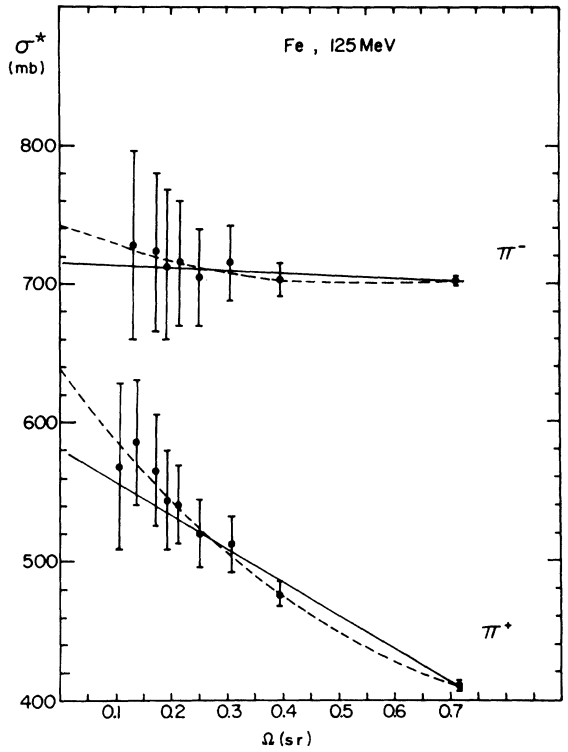

FIG. 3. The difference between the results of transmission and angular distribution experiments $\sigma^*(\Omega) = \sigma_{tr}(\Omega) - \int_{\Omega}^{4\pi} (d\sigma_{sc}/d\Omega)\, d\Omega$ as a function of Ω for Fe at 125 MeV. Linear (solid) and quadratic (dashed) fits to the data are used for extrapolation to $\Omega = 0$.

IV. DISCUSSION

A. Inclusive inelastic scattering

The differential cross section for pion scattering, as displayed in Fig. 2, can be characterized by two main processes: At the forward angles, the cross section is dominated by elastic scattering. The dashed line represents the calculated elastic scattering cross sections (see Appendix). Because of the finite angular resolution, the structure of the angular distribution is smeared out. At backward angles the cross section is almost totally inelastic and the shape of the angular distribution there follows the shape of the

free pion-nucleon scattering. This similarity suggests that the scattering to backward angles can be described as a quasifree process. This hypothesis is supported by the shape of the energy spectrum measured for pions scattered to backward angles.[3] The solid line in the figure is the sum of the cross sections for π^+p and π^-p (the latter being equal to π^+n) scattering,[21] normalized to the data for $\theta > 90°$. The pion-nucleon cross sections are taken at the same laboratory energy (see Ref. 23). The normalization factor N_{eff} is a measure of the effective number of nucleons which participate in the process. Since in this energy region the π^+p cross section is much larger than the π^+n cross section, N_{eff} will be related to the protons in the target nucleus, for π^+ scattering. For π^- scattering, the same argument will relate N_{eff} to the neutrons. This affinity of N_{eff} to Z for π^+ and to $(A-Z)$ for π^- scattering is demonstrated in Fig. 4. The values of N_{eff} are plotted against the proton number (Z) of the target for π^+ scattering and against the neutron number $(A-Z)$ for π^- scattering. It is evident that both follow the same dependence.

The energy dependence of N_{eff}, shown in Fig. 5, has almost the same shape for all targets. These results can be interpreted as reflecting the behavior of the mean free path of the pion in the nucleus for the scattering process. As has been shown by Hufner and Thies,[7] this mean free path is determined mainly by the true absorption reaction.

The angle-integrated inelastic scattering cross section can be obtained from the results of the present work in two ways, both of which rely on calculations of the elastic scattering process. One way is to subtract the elastic scattering differential cross section from the inclusive scattering (elastic and inelastic) differential cross section

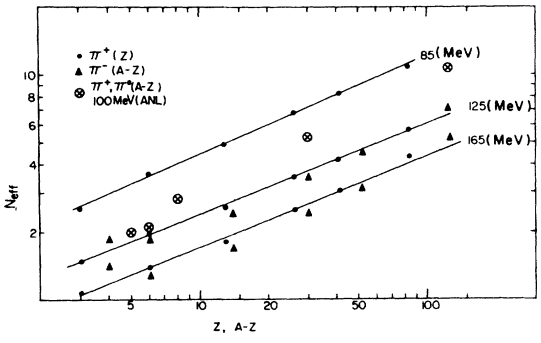

FIG. 4. N_{eff} obtained from π^+ scattering plotted against the proton number Z (circles) and from π^- scattering plotted against the neutron number $A-Z$ (triangles). The straight lines are obtained by least-squares fits to power laws. Also shown are N_{eff} values deduced from the (π^+, π^0) results of Ref. 24.

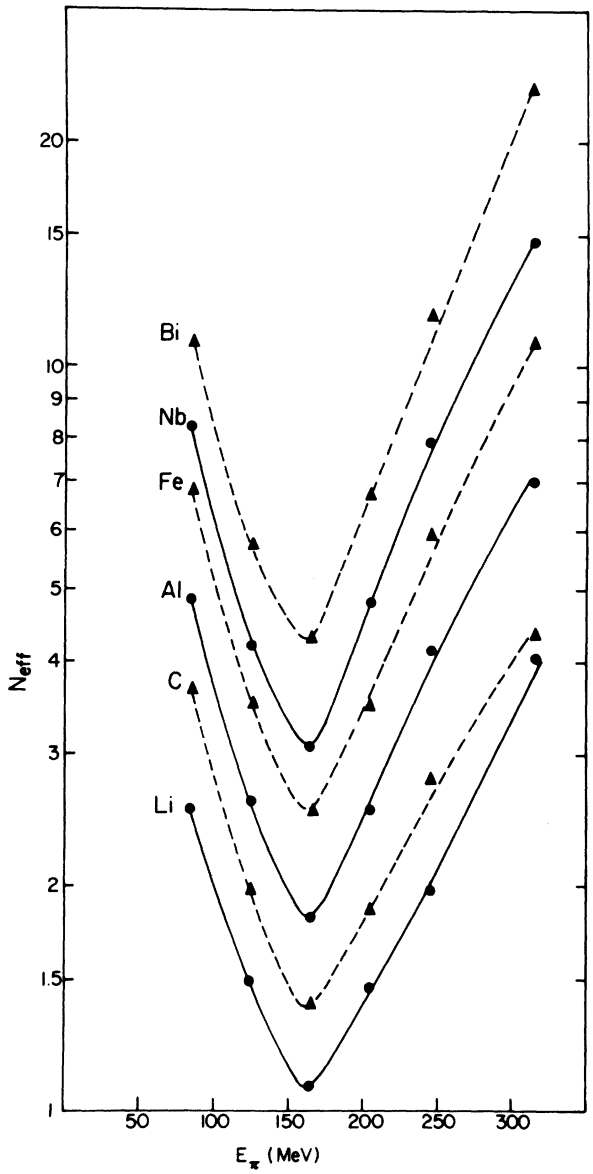

FIG. 5. Values of N_{eff} for positive pions for all studied targets as a function of bombarding energy. The lines are drawn to guide the eye.

measured in this work and integrate the difference The other way is to subtract the angle-integrated elastic scattering and the sum of absorption and charge exchange cross sections, measured in this work, from the tctal cross section (neglecting the small double charge exchange cross section):

$$\sigma_{\text{inel}} = \sigma_{\text{tot}} - \sigma_{\text{el}} - (\sigma_{\text{abs}} + \sigma_{\text{cx}}) . \quad (2)$$

While for light nuclei, both procedures can be used and, indeed, yield similar results, for heavier nuclei the first procedure has to be abandoned because of its sensitivity to the steep slope of the elastic scattering cross section at forward angles.

TABLE I. Values of N_{eff}, total pion nucleus cross sections (Ref. 1) and cross sections for true absorption, inelastic scattering, elastic scattering (calculated—see Appendix) and charge exchange (estimated—see Sec. IV B) reactions.

E_π (MeV)	Nucl.	N_{eff}	$\sigma_{abs}+\sigma_{cx}$ (mb)	σ_{cx} [a] (mb)	σ_{abs} (mb)	σ_{tot} [b] (mb)	σ_{el} [c] (mb)	σ_{inel} (mb)
85	Li	2.53	75 ± 13	31 ± 15	44 ± 20	260 ± 4	111 ± 11	74 ± 18
π^+	C	3.67	144 ± 15	35 ± 12	109 ± 20	465 ± 12	178 ± 18	143 ± 26
	Al	4.88	307 ± 29	55 ± 27	252 ± 40	1010 ± 30	372 ± 37	331 ± 56
	Fe	6.79	500 ± 55	79 ± 40	421 ± 70	1900 ± 80	616 ± 61	784 ± 115
	Nb	8.29	905 ± 100	100 ± 50	805 ± 143	2570 ± 300	817 ± 160	848 ± 350
	Bi	10.81	1800 ± 650	141 ± 70	1659 ± 655	4200 ± 600	1220 ± 240	1180 ± 920
125	Li	1.49	157 ± 16	43 ± 21	114 ± 26	425 ± 8	137 ± 14	131 ± 23
π^+	C	1.97	204 ± 23	38 ± 12	166 ± 26	638 ± 10	221 ± 22	213 ± 33
	Al	2.58	398 ± 40	58 ± 29	340 ± 50	1140 ± 40	400 ± 40	342 ± 70
	Fe	3.52	610 ± 61	83 ± 41	527 ± 74	1915 ± 80	661 ± 70	644 ± 123
	Nb	4.21	1030 ± 130	105 ± 52	925 ± 140	2580 ± 150	898 ± 180	652 ± 270
	Bi	5.73	1400 ± 220	165 ± 82	1235 ± 230	4080 ± 400	1420 ± 280	1257 ± 535
125	Li	1.85	154 ± 18	37 ± 15	117 ± 22	500 ± 9	161 ± 16	185 ± 26
π^-	C	1.86	253 ± 24	46 ± 20	207 ± 30	673 ± 14	244 ± 24	176 ± 37
	Al	2.48	464 ± 39	50 ± 25	414 ± 46	1134 ± 40	465 ± 47	205 ± 73
	Fe	3.56	728 ± 61	80 ± 40	648 ± 70	1948 ± 80	822 ± 82	398 ± 130
	Nb	4.51	1035 ± 93	100 ± 50	935 ± 100	2735 ± 200	1190 ± 240	510 ± 330
	Bi	7.11	1450 ± 300	138 ± 70	1312 ± 310	5088 ± 400	2140 ± 430	1498 ± 660
165	Li	1.07	170 ± 20	46 ± 23	124 ± 30	495 ± 8	134 ± 14	191 ± 26
π^+	C	1.39	240 ± 28	46 ± 23	194 ± 36	670 ± 8	223 ± 22	207 ± 33
	Al	1.81	410 ± 44	72 ± 36	338 ± 57	1130 ± 40	411 ± 41	321 ± 72
	Fe	2.53	680 ± 71	103 ± 50	577 ± 87	1840 ± 80	686 ± 70	474 ± 130
	Nb	3.08	1010 ± 146	130 ± 65	880 ± 160	2500 ± 150	938 ± 180	552 ± 280
	Bi	4.32	1750 ± 270	196 ± 100	1585 ± 280	3950 ± 300	1504 ± 300	696 ± 500
165	Li	1.41	160 ± 34	39 ± 16	121 ± 37	556 ± 9	159 ± 16	237 ± 40
π^-	C	1.27	249 ± 26	45 ± 20	204 ± 33	684 ± 9	242 ± 24	193 ± 37
	Al	1.69	449 ± 47	50 ± 25	399 ± 70	1122 ± 40	466 ± 47	207 ± 78
	Fe	2.43	741 ± 73	70 ± 35	671 ± 80	1868 ± 80	823 ± 82	304 ± 136
	Nb	3.13	864 ± 80	120 ± 60	744 ± 100	2725 ± 170	1186 ± 240	675 ± 300
	Bi	5.26	1220 ± 250	170 ± 85	1050 ± 265	4904 ± 300	2107 ± 420	1577 ± 570
205	Li	1.46	113 ± 20	54 ± 27	59 ± 33	462 ± 4	119 ± 12	230 ± 24
π^+	C	1.85	202 ± 29	45 ± 23	157 ± 37	626 ± 6	214 ± 21	210 ± 51
	Al	2.53	385 ± 48	58 ± 30	327 ± 57	1065 ± 35	411 ± 41	269 ± 72
	Fe	3.50	690 ± 76	83 ± 40	607 ± 86	1750 ± 70	700 ± 70	360 ± 125
	Nb	4.79	815 ± 76	130 ± 65	685 ± 100	2400 ± 120	967 ± 200	618 ± 250
	Bi	6.76	1210 ± 97	260 ± 130	950 ± 160	3840 ± 300	1570 ± 310	1060 ± 440
245	Li	1.97	92 ± 16	50 ± 25	42 ± 30	394 ± 3	93 ± 9	209 ± 19
π^+	C	2.78	142 ± 22	47 ± 23	95 ± 32	552 ± 7	186 ± 20	224 ± 30
	Al	4.13	282 ± 34	64 ± 32	218 ± 47	960 ± 35	382 ± 38	296 ± 62
	Fe	5.92	506 ± 50	95 ± 50	411 ± 70	1610 ± 70	674 ± 70	430 ± 110
	Nb	7.91	610 ± 61	170 ± 85	440 ± 105	2250 ± 120	950 ± 200	690 ± 240
	Bi	11.68	1130 ± 90	276 ± 140	854 ± 166	3810 ± 200	1580 ± 320	1100 ± 390
315	Li	4.04	40 ± 33			288 ± 4	60 ± 6	188 ± 34
π^+	C	4.34	109 ± 16	45 ± 22	64 ± 27	445 ± 7	136 ± 14	200 ± 22
	Al	6.98	192 ± 25	73 ± 36	119 ± 44	810 ± 35	311 ± 32	307 ± 54
	Fe	10.67	418 ± 36	98 ± 50	320 ± 62	1400 ± 70	593 ± 60	389 ± 100
	Nb	14.73	544 ± 44	154 ± 80	390 ± 90	2000 ± 120	877 ± 180	579 ± 220
	Bi	23.5	922 ± 77	304 ± 150	618 ± 170	3500 ± 200	1550 ± 310	1028 ± 380

[a] Estimated—see Sec. IV B.
[b] From Ref. 1.
[c] Calculated—see Appendix.

We therefore prefer to use the second procedure, which needs only angle-integrated cross sections and is, therefore, also less sensitive to details of the elastic scattering calculations. The procedures used for these calculations are described in the Appendix and, as is shown, the agreement with available elastic scattering data is quite good. The results of these calculations are given in Table I. For total cross sections, we used the results of Carroll *et al.*[1] with some interpolation to fit the nuclei and bombarding energies studied in this work. The values used are listed in Table I. Then, through the relationship (2), the inclusive inelastic scattering cross section is obtained and listed in Table I. Since the value of σ_{inel} is obtained by subtraction of σ_{el} and $\sigma_{abs}+\sigma_{cx}$ from σ_{tot} [Eq. (2)], the errors in these values propagate into the uncertainty in σ_{inel}. In light and medium-heavy nuclei σ_{tot} is known quite precisely. With typical errors of 10–15% in the two other values, the error in σ_{inel} becomes typically 20–30%. The situation becomes worse in the heavy nuclei where all the errors become considerably larger.

If the inclusive inelastic scattering cross section is predominantly due to quasifree scattering, one would expect to have $\sigma_{inel} = N_{eff}\sigma(\pi N)$. In Fig. 6, we plot the ratio $B(A,E) = \sigma_{inel}/N_{eff}\sigma(\pi N)$ for positive pions; the values for negative pions are very similar. We note that at the higher energies this ratio is fairly constant, independent of energy and A, with a value of 0.6–0.8. This indicates that at forward angles the cross section for inelastic scattering becomes considerably smaller than that for free pion-nucleon scattering normalized to the data at backward angles. These ratios, therefore, reflect the effect of Pauli blocking.[6] Even inelastic scattering to specific final nuclear states, which is sometimes forward peaked, does not compensate this blocking effect. At lower energies, we note that for heavy targets this ratio becomes very large. This may have either of the following explanations: Because of the great difficulties in making the Coulomb corrections for extracting σ_{tot}, there are large errors in these values for the heavy targets. Although these are taken into account in Fig. 6, some systematic errors in σ_{tot} could cause this effect. Alternatively, if this effect or part of it is genuine, then, perhaps, the inelastic scattering to low lying states, giant resonances, etc., for heavy elements and at lower energies, more than compensates for the effect of the Pauli blocking. This question will have to be settled by experiments in which the inclusive inelastic scattering is directly measured at forward angles.

The energy dependence of the inclusive inelastic scattering cross section shows a rise with energy (for light nuclei) below the resonance, but above the resonance the cross section remains practically constant. The shape of the resonance is not reflected much in this process. The A dependence of this cross section is weaker than for any other reaction (see Figs. 9 and 10).

B. Estimate of the single charge exchange cross section

As was stated in Sec. III, the quantity measured in this work is the sum of cross sections for true absorption and single charge exchange reactions $\sigma_{abs}+\sigma_{cx}$. It turns out that in most cases the value of σ_{cx} is a relatively small part (~15%) of this measured quantity and, therefore, even a crude estimate of this cross section will allow us to extract the cross sections for true absorption with reasonable precision. In this section, we describe the procedure used to estimate σ_{cx}, and we emphasize that this is done only for the extraction of σ_{abs} and not for any quantitative conclusions regarding the single charge exchange process. The need to make estimates of σ_{cx} is a result of the scarcity of experimental data on this reaction. A summary of the available data on this cross section is given in Table II.

The inclusive single charge exchange cross section was recently measured by Bowles *et al.*[24,25] Their results show that the shape of the angular distribution for the inclusive (π^+,π^0) reaction on ^{16}O and ^{58}Ni at 100 MeV is very similar to that of the inclusive inelastic scattering. By normalizing their data to the free pion nucleon charge exchange cross section, an N_{eff} value is deduced. In Fig. 4 we plot the values of N_{eff} deduced from these measurements[24](together with those obtained in the present work). They are plotted against $(A-Z)$ since the (π^+,π^0) reaction acts on the neutrons in the target. It is evident from this figure that the inclusive charge exchange reaction follows a pattern similar to that of the inclusive inelastic scat-

TABLE II. Summary of available experimental data on inclusive single charge exchange cross sections together with the corresponding values calculated as described in Sec. IV B.

Target	E_π	Cross section (mb) measured	calculated	Ref.
C	70	27.5 ± 8.7	34	27
Al	70	39.5 ± 12.4	44	27
Cu	70	44.3 ± 14	64	27
Pb	70	58.7 ± 19	96	27
^{16}O	100	66 ± 10	56	25
^{9}Be	100	45 ± 7	38	25
^{28}Ni	100	104 ± 15	92	25
^{12}C	130	36 ± 5	50	26

tering. The values of N_{eff} obtained from the charge exchange reaction are in very good agreement with those deduced from the inelastic scattering. This similarity leads us to base the estimate of σ_{cx} on the inclusive inelastic scattering data. In order to do that, we note, first, that while the N_{eff} obtained from inelastic scattering of positive pions is a measure of the effective number of protons participating in the process, for the (π^+, π^0) reaction the effective number of neutrons is required. In order to get this number, we use the fact that the proton and neutron values of N_{eff} have the same Z and $(A-Z)$ dependence, respectively (Fig. 4). We, therefore, can get the neutron N_{eff} value for the (π^+, π^0) reaction from the proton N_{eff} and its power law dependence (see Sec. IV D). We also assume that the charge exchange reaction suffers from the same "blocking" as the inelastic scattering. The estimated value of σ_{cx} can, therefore, be written

$$\sigma_{cx}(A,E)_{\text{est}} = B(A,E)\cdot N_{\text{eff}}(A,E)\cdot\left(\frac{A-Z}{Z}\right)^{q(E)}\sigma(\pi^- p\to\pi^0 n), \quad (3)$$

where $\sigma(\pi^- p\to\pi^0 n)$ is taken from Ref. 28, $B(A,E)$ is the blocking parameter taken from Fig. 6, and $q(E)$ is the power law for N_{eff} discussed in Sec. IV D. We must, however, make an exception from this procedure for the heavy elements at low energies. For these cases, Fig. 6 shows very large values of B which, as discussed in Sec. IV A, might even be wrong and carry very large errors. In any case, we can see that the value of B that should be used in Eq. (3) for such cases is much smaller: The measured value of σ_{cx} for ^{58}Ni at 100 MeV is 104 mb. If we take B (from Fig. 6) as 2.2, the value of σ_{cx} estimated by Eq. (3) is 224 mb. A value of B of the order of unity will yield good agreement with the data. Since at the higher energies B is A independent, we take B for the low energies (85 and 125 MeV) from the light nuclei to be 0.8. In Table II, we list charge exchange cross sections, calculated for the cases where measurements exist, and the agreement is fairly good. Finally, we note that since for ^{12}C there are some measured values of σ_{cx} at 70, 100, and 130 MeV (Table II), we can use these values with some interpolation for 85 and 125 MeV.

Since this procedure is rather crude, we assign a large error, 50%, to the estimated values of σ_{cx}. The errors assigned to σ_{cx} for ^{12}C at 85 and 125 MeV are smaller, 30%, since for these cases experimental values already exist.

C. The true absorption cross section

The values of σ_{cx}, estimated according to the procedure described in the previous section, are subtracted from the quantities measured in the present work, $\sigma_{abs}+\sigma_{cx}$, and the absorption cross section is obtained. Since in most cases σ_{cx} is small compared with the measured quantity, even with the assignment of a large error (50%) to the estimated value of σ_{cx}, the final error in σ_{abs} is kept in the range of 15–20%. For the light nuclei σ_{cx} is relatively larger, especially at energies far from the resonance. Measurements of σ_{cx}, in particular for light nuclei, with precision of 20–30%, will enable the reduction of the errors in σ_{abs}. In some cases (see Sec. IV B), these measurements were done and, indeed, helped to reduce the errors. The resulting values of σ_{abs} are listed in Table I and plotted in Fig. 7. The general trend is similar to that of the total cross section.[1]

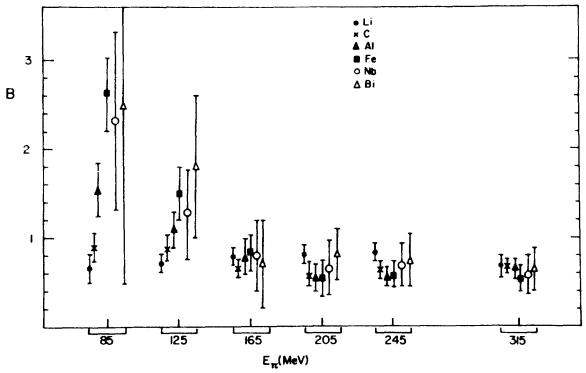

FIG. 6. Values of $B(A,E)=\sigma_{\text{inel}}/N_{\text{eff}}\cdot\sigma(\pi N)$ for all targets and bombarding energies.

Theoretical calculations of the absorption cross section were carried out by several authors. In Fig. 8, the measured cross sections for pion absorption in ^{12}C are compared to calculations. To calculate the cross section, one starts from some absorption strength and then develops a method of following the pion in the nucleus to obtain the absorption probability. The various groups used different approaches which will be mentioned briefly. Ginocchio and Johnson[5] (dashed line) used pion production data for the absorption strength, followed by cascade calculations. Lenz[6] (solid line) obtained an absorption width from $\pi - {}^4$He scattering and applied it to optical model calculations. Hüfner and Thies[7] (dashed-dot line) used a similar width and developed a transport calculation method to follow the pion in the nucleus. Agassi and Koltun also reported[8] transport calculations which follow the Δ isobar in the nucleus. Stricker *et al.*[9] (dotted line) derive their absorption parameters from pionic atom data. In general, the calculations reproduce the magnitude of the cross section reasonably well, but the agreement between the calculated and measured energy

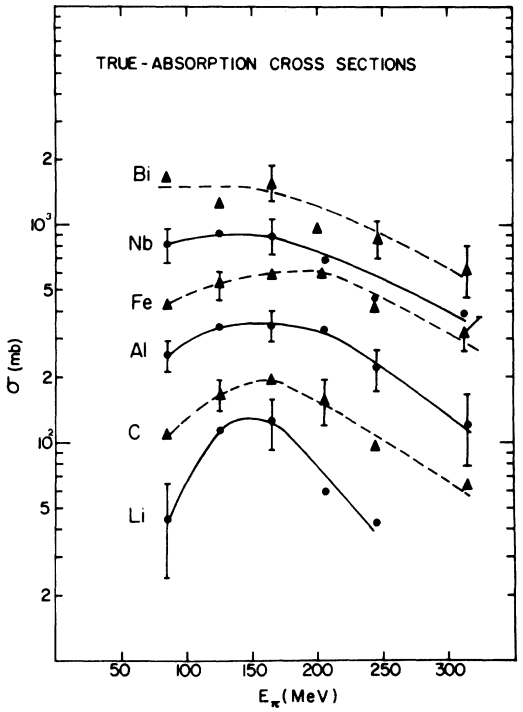

FIG. 7. The true absorption cross sections of π^+ for all the studied target nuclei, as a function of bombarding energy. The lines are drawn to guide the eye and typical error bars are shown.

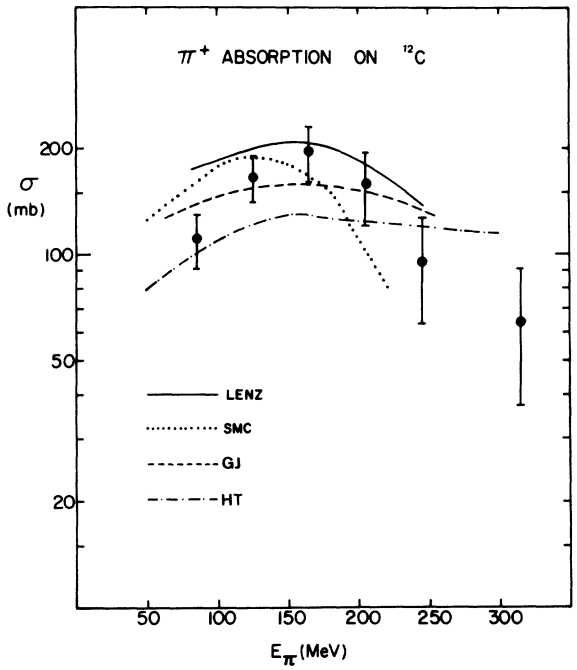

FIG. 8. True absorption cross section of positive pions on carbon compared to calculations: dashed line—Ref. 5; solid line—Ref. 6; dashed-dot line—Ref. 7; and dotted line—Ref. 9.

dependence of the cross section is poor. The experimental results show a much stronger energy dependence than theoretically expected. The shape of the resonance is reflected in the absorption cross section much more than in any other reaction. Above the resonance, while the inclusive inelastic scattering remains constant, the absorption cross section drops rapidly (see Fig. 11). The A dependence of the absorption cross section is steeper than that of the inclusive inelastic scattering (see Fig. 9). As a result, the absorption process takes an increasing fraction of the reaction cross section as we go to heavier nuclei, and in the center of the resonance region it is the dominant reaction in heavy nuclei. This generally steep A dependence was correctly predicted by Ginocchio[12].

It is interesting to note that when the absorption cross section is extrapolated to $A = 2$, the result is 4–5 times greater than the absorption cross section on the deuteron.[11] This reflects the low nuclear density of the deuteron and the availability of absorption channels and mechanisms other than the $(\pi^+, 2p)$ or $(\pi^-, 2n)$ for heavier nuclei.

Comparison of the cross sections for positive and negative pion absorption shows that, at the two bombarding energies where it was measured (125 and 165 MeV), they are generally similar. We may expect two compensating effects in this comparison: Coulomb attraction can increase the absorption of negative pions, while for the heavy neutron rich nuclei the probability of positive pion absorption will be enhanced. At 125 MeV, we observe that in the heavy nuclei the cross sections

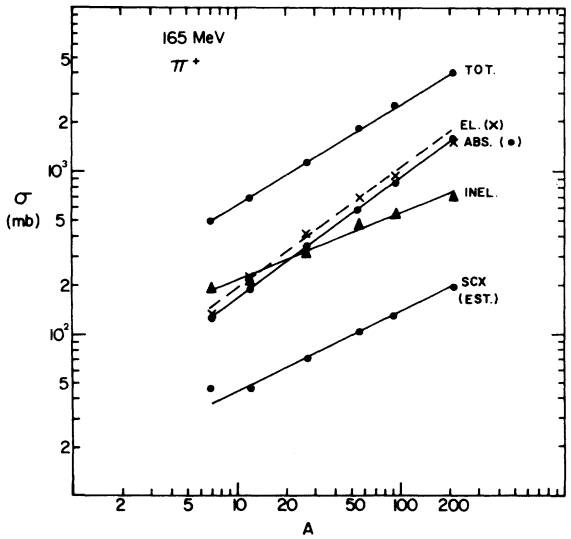

FIG. 9. Decomposition of the total π^+-nucleus cross section at 165 MeV. The lines are least squares fits to power laws.

for positive and negative pion absorption are about equal, i.e., the effects compensate for each other, while for medium heavy nuclei π^- absorption is larger. At 165 MeV, the effect of Coulomb attraction is relatively smaller and π^+ absorption in the heavy neutron rich nuclei is stronger than for π^-.

D. Decomposition of the cross section

By combining the results of the present work with measurements of total cross sections and with calculations and measurements of elastic scattering cross sections, it is possible to decompose the total pion-nucleus cross section into its major channels. This decomposition can help in better understanding the reactive content of the pion nucleus interaction. An illustration of this decomposition is given in Fig. 9, where the elastic scattering, inclusive inelastic scattering, and true absorption cross sections are plotted against the nuclear mass number for a fixed bombarding energy. Also shown are the estimated cross sections for the single charge exchange reaction. The cross sections are seen to lie on straight lines in the log-log plot, which represents an A dependence through power laws. It appears to be useful,

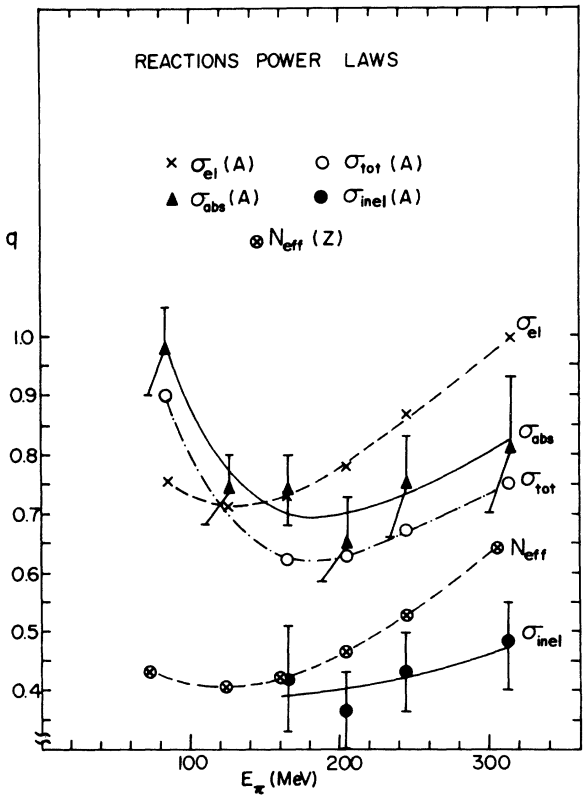

FIG. 10. Exponents of least squares fits to power laws for the cross sections as a function of A and of N_{eff} as a function of Z for positive pions. The lines are drawn to guide the eye.

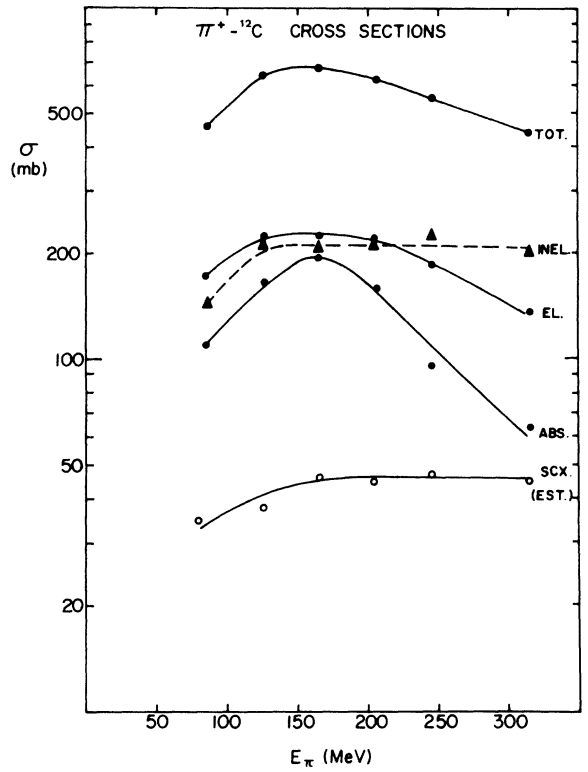

FIG. 11. Decomposition of the total π^+-carbon cross section. The lines are drawn to guide the eye.

then, to parametrize the cross sections through power laws of the type

$$\sigma_m = P_m(E)A^{q_m(E)} .$$

The values of the exponents $q_m(E)$ obtained by a least-square fit to the data are shown in Fig. 10. It can be noted that between the two major reaction channels—the inclusive inelastic scattering and the true absorption—the latter always takes a much steeper A dependence with an exponent of about twice that of the former. This may be interpreted as reflecting geometrical effects due to the different regions in the nuclear volume and surface where the reactions take place. Alternatively, this effect may be related to the interpretation of the inelastic scattering as an interaction with single nucleons compared to the absorption process which is involved with nucleon pairs. It is expected that these power-law parametrizations will be useful both as a guideline for understanding the reaction mechanisms and as a practical way for performing interpolations. Also shown in Fig. D are the exponents for $N_{\rm eff} = P(E)Z^{q(E)}$. This should be useful since at backward angles we have

$$\left(\frac{d\sigma}{d\Omega}\right)_{\rm inel} = N_{\rm eff} \times [\sigma(\pi^+ p) + \sigma(\pi^+ n)] .$$

In Fig. 11 we show the decomposition of the total cross section into the major channels for ^{12}C as a function of the bombarding energy. It may be seen here that the energy dependence of the absorption cross section is stronger than for the other reactions and reflects the shape of the resonance, while the inelastic scattering remains practically constant.

Theoretical calculations of the partial cross sections and ways to decompose the reactive content of the pion nucleus interaction were described by several authors. These include separating the imaginary part of the optical potential into absorptive and scattering components,[7] or dealing with scattering and absorptive mean-free paths.[7,10] It is hoped that through the comparison of these calculations with the experimental results presented here, our understanding of the reactive content will be improved. Since both the scattering and absorption cross sections are large, particularly at the resonance, coupling between the two is expected to exist. As was pointed out by Hüfner and Thies,[7] the scattering mean-free path is strongly affected by the magnitude of the absorption cross section. Experimentally, this coupling was demonstrated recently[18,29] by the study of pion scattering and absorption on ^{16}O and ^{18}O.

ACKNOWLEDGMENTS

It is a pleasure to thank Dr. F. Lenz, Dr. E. Moniz, Dr. J. Eisenberg, Dr. D. Koltun, Dr. J. Schiffer, and Dr. H. Jackson for many illuminating discussions. The authors from Tel Aviv University are grateful for the warm hospitality of the SIN laboratory. We thank Mr. A. Altman, E. Piasetzky, and M. Zilca for their participation during parts of the experiments. The skillful technical assistance of Mr. E. Hermes is deeply acknowledged. This work was supported in pary by the Israeli commission for Basic Research and by the Swiss Institute for Nuclear Research.

APPENDIX: ELASTIC SCATTERING CALCULATIONS

To estimate the total angle-integrated elastic cross sections, calculations based on the first-order Kisslinger potential were performed using the code PIRK[30]. The parameters of the potential were obtained from an isospin average of the free πN amplitudes.[31] The charge density parameters were taken from a compilation of electron-scattering results,[32] and the nuclear density parameters were set equal to them. Although this model is very crude and does not use parameters from fitted cross sections, it has the advantage of defining a procedure that can be used to study the systematic dependence of the elastic cross section on a full range of incident pion energies and targets.

The reliability of these calculations was tested by comparing them to elastic scattering data. The general features of the differential cross sections were well reproduced for E_π near the resonance. The elastic cross sections were also integrated over the range of measured data, and the comparison of experiment with theory, presented in Table III, was generally found to be good. For $E_\pi < 90$ MeV, the results presented in Table III are from calculations based on a second-order optical potential, with the parameters interpolated from those obtained from pionic atom data by Stricker, McManus, and Carr.[9] That potential was shown to be well suited for low-energy elastic scatter-

TABLE III. Angle-integrated elastic scattering data and calculations. θ_{min} is the most forward angle for which the elastic scattering was measured. The experimental data is integrated from θ_{min} to 180° and the same integration is performed for the calculation. Also shown is σ_{el}, the complete angle integrated cross section.

Target	E_π (MeV)	θ_{min}	$\int_\theta^{180}$ (exp)	$\int_\theta^{180}$ (calc)	σ_{el}	Ref.
^{12}C	87.5, π^-	25	113	109	210	33
^{12}C	120, π^-	10	224	216	243	34
^{12}C	162, π^+	10	205	189	223	35
^{12}C	162, π^-	13	175	161	242	35
^{12}C	230, π^-	10	152	149	216	34
^{12}C	260, π^-	10	152	129	195	34
^{28}Si	162, π^+	14	240	223	418	36
^{40}Ca	116, π^+	14	338	319	513	37
^{40}Ca	116, π^-	14	381	353	621	37
^{40}Ca	162, π^-	14	226	255	547	37
^{58}Ni	162, π^+	14	279	287	692	36
^{208}Pb	116, π^+	14	646	729	1425	38
^{208}Pb	116, π^-	14	648	655	2190	38
^{208}Pb	162, π^+	14	354	439	1507	36
^{208}Pb	162, π^-	16	212	203	2126	36

ing.[9] The code used was a modified version of PIRK[30].

The nuclear part of the elastic scattering was obtained by removing the Coulomb and Coulomb-nuclear interference terms from the differential cross sections. The total elastic cross section

$$\sigma_{el} = \frac{\pi}{k^2} \sum_l (2l+1)|1 - S_l|^2$$

is also presented in Table III to show the "missing" part of the integrated nuclear elastic cross section at forward angles. Furthermore, at very forward angles, the Coulomb and Coulomb-nuclear interference contributions to the elastic cross sections become dominant, and one must rely entirely on the calculation for the nuclear part. Using this prescription, we assume that the error of the nuclear elastic cross section at forward angles is not much bigger than at backward angles. By comparing the results of the calculations with experimental data (Table III), we can estimate the precision of the calculations. The adopted uncertainties in the calculations are 10% for the mass range Li-Fe and 20% for Nb and Bi. For the latter, in particular, the Coulomb terms are very large even at backward angles.

---

*Present address: TRIUMF, Vancouver, Canada.
†Present address: ASK, CH-5303, Wurenlingen, Switzerland.

[1]A. S. Carroll, I. H. Chiang, C. B. Dover, T. F. Kycia, K. K. Li, P. O. Mazur, D. N. Michael, P. M. Mockett, D. C. Rahm, and R. Rubinstein, Phys. Rev. C 14, 635 (1976).
[2]E. Boschitz, *Seventh International Conference on High Energy Physics and Nuclear Structure*, edited by M. P. Locher (Birkhäuser, Zurich, 1977), p. 133.
[3]C. H. Q. Ingram, in *Meson-Nuclear Physics-1979 (Houston)*, Proceedings of the Second Conference on Meson-Nuclear Physics, edited by E. V. Hungerford (AIP, New York, 1979), p. 455.
[4]J. M. Eisenberg, see Ref. 3, p. 1.
[5]J. N. Ginocchio and M. B. Johnson, Phys. Rev. C 21, 1056 (1980).
[6]F. Lenz, Proceedings of the Topical Meeting on Intermediate Energy Physics, Zuoz, 1976, Vol. 2, p. 319.
[7]J. Hufner and M. Thies, Phys. Rev. C 20, 273 (1979).
[8]D. Agassi and D. S. Koltun, see Ref. 3, p. 601.
[9]K. Stricker, H. McManus, and J. A. Carr, Phys. Rev. C 19, 929 (1979).
[10]K. S. Koltun, see Ref. 3, p. 87.
[11]C. Richard-Serre, W. Hirt, D. F. Measday, E. G. Michaelis, M. J. M. Saltmarsch, and P. Skarek, Nucl. Phys. B20, 413 (1970).
[12]J. N. Ginocchio, Phys. Rev. C 17, 195 (1978).
[13]E. Bellotti, D. Cavalli, and C. Matteuzzi, Nuovo Cimento 18A, 75 (1973).
[14]D. I. Sober, W. J. Briscoe, P. E. Burt, H. Crannel, J. T. O'Brien, and W. J. Stapor, Phys. Rev. C 21, 1465 (1979).
[15]I. Navon, D. Ashery, G. Azuelos, H. J. Pfeiffer, H. K. Walter, and F. W. Schlepütz, Phys. Rev. Lett. 42, 1465 (1979).
[16]I. Navon, D. Ashery, G. Azuelos, H. J. Pfeiffer, H. K. Walter, and F. W. Schlepütz, see Ref. 3, p. 535.
[17]I. Navon, D. Ashery, G. Azuelos, H. J. Pfeiffer, H. K. Walter, and F. W. Schleputz, in Proceedings of the Eighth Conference on High Energy Physics and Nuclear Structure, Vancouver, 1979, edited by D. F. Measday (AIP, New York, to be published), p. 48.
[18]D. Ashery, Nucl. Phys. A335, 385 (1980).
[19]I. Navon, D. Ashery, G. Azuelos, H. J. Pfeiffer, H. K. Walter, and F. W. Schlepütz, Phys. Rev. C 22, 217 (1980).
[20]I. Navon, Ph.D. thesis, Tel Aviv University, 1980.
[21]P. J. Bussey, J. R. Carter, D. R. Dance, D. V. Bugg, A. A. Carter, and A. M. Smith, Nucl. Phys. B58, 363 (1973).
[22]C. W. Bjork, S. E. Jones, T. R. King, D. M. Manley, A. T. Oyer, G. A. Rebka, J. B. Walter, R. Carawon, P. A. M. Gram, F. T. Shively, C. A. Bordner, and E. L. Lomon, Phys. Rev. Lett. 44, 62 (1980).
[23]S. A. Gurvitz, J. P. Dedonder, and R. D. Amado, Phys. Rev. C 19, 142 (1979).
[24]T. J. Bowles, D. F. Geesaman, R. J. Holt, H. E. Jackson, R. M. Lawzewski, J. R. Specht, L. L. Rutledge, R. E. Segel, R. P. Redwine, and M. A. Yates-Williams, Phys. Rev. Lett. 40, 97 (1978).
[25]T. J. Bowles, D. F. Geesman, R. J. Holt, H. E. Jackson, J. Julien, R. M. Laszewski, J. R. Specht, E. J. Sleptenson, R. P. Redwine, L. L. Rutledge, R. E. Segel, and M. A. Yates, Phys. Rev. C 23, 439 (1981).
[26]E. Bellotti, S. Bonetti, D. Cavalli, and C. Matteuzzi, Nuovo Cimento 14A, 567 (1973).
[27]H. Hilscher, W. D. Krebs, G. Sepp, and V. Soergel, Nucl. Phys. A158, 602 (1970).
[28]D. V. Bugg, P. J. Bussey, D. R. Dance, A. R. Smith, A. A. Carter, and J. R. Williams, Nucl. Phys. B26, 588 (1971).
[29]I. Navon, E. Piasetzky, D. Ashery, A. Altman, F. W. Schlepütz, and H. K. Walter, Phys. Lett. 95B, 365 (1980).
[30]R. A. Eisenstein and G. A. Miller, Comp. Phys. Comm. 8, 130 (1974).
[31]CERN phase shifts, Report No. VCRL-20030πN, Lawrence Radiation Laboratory, Berkeley, 1970.
[32]C. W. de Jager, H. de Vries, and C. de Vries, At. Data Nucl. Data Tables 14, 479 (1974).
[33]R. M. Edelstein, W. F. Baker, and J. Rainwater, Phys. Rev. 122, 252 (1961).
[34]F. Binon, P. Duteil, J. P. Garon, J. Gorres, L. Hugon, J. P. Peigneux, C. Schmit, M. Spighel, and J. P. Stroot, Nucl. Phys. B17, 168 (1970).
[35]H. A. Thiessen, in MP-10 Progress Report, Los Alamos Scientific Laboratory, 1978; J. Piffaretti, R. Corfu, J. P. Egger, P. Gretillat, C. Lunke, E. Schwarz, C. Perrin, and B. M. Preedom, Phys.

Lett. 71B, 324 (1977).
[36]B. Zeidman, C. Olmer, D. F. Geesaman, R. L. Boudrie, R. H. Siemssen, J. F. Amman, C. L. Morris, H. A. Thiessen, G. R. Burleson, M. J. Devereux, R. E. Segel, and L. W. Swenson, Phys. Rev. Lett. 40, 1316 (1978); B. Zeidman, private communication.
[37]Q. Ingram, E. Boschitz, L. Pflug, J. Zichy, J. P. Albanese, and J. Arvieux, Phys. Lett. 76B, 173 (1978).
[38]J. Arvieux, J. P. Albanese, J. Bolger, E. Boschitz, C. H. O. Ingram, L. Pflug, J. Jansen, and J. Zichy, Nucl. Phys. A312, 368 (1978).